

## Slow Magnetic Relaxation in a Family of Trigonal Pyramidal Iron(II) Pyrrolide Complexes

W. Hill Harman,<sup>†,§</sup> T. David Harris,<sup>†</sup> Danna E. Freedman,<sup>†</sup> Henry Fong,<sup>†</sup>  
 Alicia Chang,<sup>†</sup> Jeffrey D. Rinehart,<sup>†</sup> Andrew Ozarowski,<sup>#</sup> Moulay T. Sougrati,<sup>||</sup>  
 Fernande Grandjean,<sup>||</sup> Gary J. Long,<sup>\*,‡</sup> Jeffrey R. Long,<sup>\*,†</sup> and  
 Christopher J. Chang<sup>\*,†,‡,§</sup>

*Department of Chemistry and the Howard Hughes Medical Institute, University of California, Berkeley, California 94720, United States, Chemical Sciences Division, Lawrence Berkeley National Laboratory, Berkeley, California 94720, United States, Department of Physics, B5, University of Liège, B-4000 Sart-Tilman, Belgium, Department of Chemistry, Missouri University of Science and Technology, University of Missouri, Rolla, Missouri 65409-0010, United States, and National High Magnetic Field Laboratory, Florida State University, Tallahassee, Florida 32310, United States*

Received June 16, 2010; E-mail: chrischang@berkeley.edu; jrlong@berkeley.edu; glong@mst.edu

**Abstract:** We present a family of trigonal pyramidal iron(II) complexes supported by tris(pyrrolyl- $\alpha$ -methyl)amine ligands of the general formula  $[M(\text{solv})_n](\text{tpa}^R)\text{Fe}$  ( $M = \text{Na}$ ,  $R = \textit{tert}$ -butyl (**1**), phenyl (**4**);  $M = \text{K}$ ,  $R = \textit{mesityl}$  (**2**), 2,4,6-triisopropylphenyl (**3**), 2,6-difluorophenyl (**5**)) and their characterization by X-ray crystallography, Mössbauer spectroscopy, and high-field EPR spectroscopy. Expanding on the discovery of slow magnetic relaxation in the recently reported mesityl derivative **2**, this homologous series of high-spin iron(II) complexes enables an initial probe of how the ligand field influences the static and dynamic magnetic behavior. Magnetization experiments reveal large, uniaxial zero-field splitting parameters of  $D = -48, -44, -30, -26,$  and  $-6.2 \text{ cm}^{-1}$  for **1–5**, respectively, demonstrating that the strength of axial magnetic anisotropy scales with increasing ligand field strength at the iron(II) center. In the case of 2,6-difluorophenyl substituted **5**, high-field EPR experiments provide an independent determination of the zero-field splitting parameter ( $D = -4.397(9) \text{ cm}^{-1}$ ) that is in reasonable agreement with that obtained from fits to magnetization data. Ac magnetic susceptibility measurements indicate field-dependent, thermally activated spin reversal barriers in complexes **1**, **2**, and **4** of  $U_{\text{eff}} = 65, 42,$  and  $25 \text{ cm}^{-1}$ , respectively, with the barrier of **1** constituting the highest relaxation barrier yet observed for a mononuclear transition metal complex. In addition, in the case of **1**, the large range of temperatures in which slow relaxation is observed has enabled us to fit the entire Arrhenius curve simultaneously to three distinct relaxation processes. Finally, zero-field Mössbauer spectra collected for **1** and **4** also reveal the presence of slow magnetic relaxation, with two independent relaxation barriers in **4** corresponding to the barrier obtained from ac susceptibility data and to the 3D energy gap between the  $M_S = \pm 2$  and  $\pm 1$  levels, respectively.

### Introduction

Since the early 1990s, certain molecules have been shown to exhibit an energy barrier to magnetic relaxation, thereby enabling them to retain their magnetization after removal of an applied field and thus act as nanoscopic classical magnets.<sup>1–5</sup> This relaxation barrier arises due to a uniaxial magnetic anisotropy ( $D$ ) acting on a nonzero spin ground state ( $S$ ),

according to the expression  $U = S^2|D|$ . Complexes exhibiting this behavior, known as single-molecule magnets, have garnered considerable interest owing to their potential applications in high-density information storage, quantum computing, and magnetic refrigeration.<sup>6–15</sup> However, in order for any such applications to be realized, higher relaxation barriers must be

<sup>†</sup> Department of Chemistry, University of California, Berkeley.

<sup>‡</sup> Howard Hughes Medical Institute, University of California, Berkeley.

<sup>§</sup> Lawrence Berkeley National Laboratory.

<sup>#</sup> Florida State University.

<sup>||</sup> University of Liège.

<sup>‡</sup> University of Missouri.

- (1) Sessoli, R.; Tsai, H. L.; Schake, A. R.; Wang, S.; Vincent, J. B.; Foltling, K.; Gatteschi, D.; Christou, G.; Hendrickson, D. N. *J. Am. Chem. Soc.* **1993**, *115*, 1804.
- (2) Sessoli, R.; Gatteschi, D.; Caneschi, A.; Novak, M. A. *Nature* **1993**, *365*, 141.
- (3) Gatteschi, D.; Sessoli, R.; Villain, J. *Molecular Nanomagnets*; Oxford University Press: Oxford, 2006.

- (4) Milios, C. J.; Vinslava, A.; Wernsdorfer, W.; Moggach, S.; Parsons, S.; Perlepes, S. P.; Christou, G.; Brechin, E. K. *J. Am. Chem. Soc.* **2007**, *129*, 2754.
- (5) Yoshihara, D.; Karasawa, S.; Koga, N. *J. Am. Chem. Soc.* **2008**, *130*, 10460.
- (6) Garanin, D. A.; Chudnovsky, E. M. *Phys. Rev. B* **1997**, *56*, 11102.
- (7) Leuenberger, M. N.; Loss, D. *Nature* **2001**, *410*, 789.
- (8) Jo, M. H.; Grose, J. E.; Baheti, K.; Deshmukh, M. M.; Sokol, J. J.; Rumberger, E. M.; Hendrickson, D. N.; Long, J. R.; Park, H.; Ralph, D. C. *Nano Lett.* **2006**, *6*, 2014.
- (9) Ardavan, A.; Rival, O.; Morton, J. J. L.; Blundell, S. J.; Tyryshkin, A. M.; Timco, G. A.; Winpenny, R. E. P. *Phys. Rev. Lett.* **2007**, *98*, 57201.
- (10) Bogani, L.; Wernsdorfer, W. *Nat. Mater.* **2008**, *7*, 179.
- (11) Stamp, P. C. E.; Gaita-Arino, A. *J. Mater. Chem.* **2009**, *19*, 1718.

achieved. Indeed, despite the enormous effort aimed at generating single-molecule magnets with high relaxation barriers, to date, no molecule has shown magnetic hysteresis above 10 K.

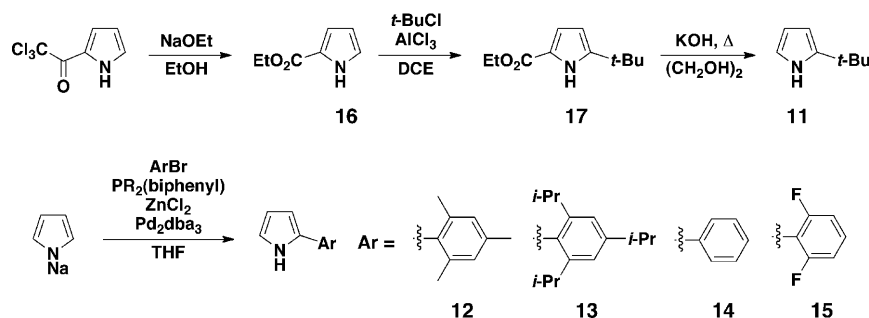
The vast majority of single-molecule magnets characterized thus far have taken the form of multinuclear transition metal cluster compounds.<sup>1–5</sup> Recently, however, researchers have uncovered slow magnetic relaxation in mononuclear lanthanide and actinide complexes.<sup>16–20</sup> In these complexes, the large spin-orbit coupling of the f-block ion gives rise to a highly anisotropic ground state. In particular, this discovery has led to mononuclear lanthanide phthalocyanine complexes with very high relaxation barriers. In principle, similar behavior should be attainable in a mononuclear transition metal complex with a high-spin ground state and uniaxial anisotropy. However, unlike their f-block counterparts that display significant spin-orbit coupling largely independent of ligand field effects, the orbital moment of transition metal coordination compounds is frequently quenched by geometric distortions.<sup>21–25</sup> Furthermore, in the absence of steric protection, transition metal ions often undergo coordinative saturation to form low-spin complexes. Thus, the task of creating mononuclear transition metal-based single-molecule magnets requires enforcing coordination geometries that preserve a high-spin ground state while minimizing or preventing anisotropy-quenching structural distortions.

This task is ideally suited to molecular inorganic chemistry and its focus on the design and synthesis of geometrically constrained and sterically bulky ligands. Indeed, many metal complexes developed within this paradigm display novel or enhanced molecular reactivity,<sup>26–30</sup> as well as atypical spin states<sup>31</sup> and bonding configurations.<sup>33,32–37</sup> Of particular promise toward the develop-

ment of single-molecule magnets are low-coordinate high-spin iron(II) complexes, some of which have been reported to show axial zero-field splitting magnitudes up to  $|D| = 50 \text{ cm}^{-1}$ ,<sup>38–43</sup> as in the case of the planar complex ( $\beta$ -diketiminate)FeCH<sub>3</sub>.<sup>38</sup> In view of these principles and the wealth of inorganic coordination chemistry carried out by iron in heme and nonheme protein active sites<sup>44</sup> and their synthetic models,<sup>45–50</sup> many laboratories, including ours, have been interested in exploring the structure, magnetism, and reactivity of iron complexes in lower-coordinate two-<sup>51–55</sup> and three-fold<sup>32,33,43,56–68</sup> environments. In this context, we have

- (12) Affronte, M.; Troiani, F.; Ghirri, A.; Candini, A.; Evangelisti, M.; Corradini, V.; Carretta, S.; Santini, P.; Amoretti, G.; Tuna, F.; Timco, G.; Winpenny, R. E. P. *J. Phys. D Appl. Phys.* **2007**, *40*, 2999.
- (13) Manoli, M.; Johnstone, R. D. L.; Parsons, S.; Murrie, M.; Affronte, M.; Evangelisti, M.; Brechin, E. K. *Angew. Chem., Int. Ed.* **2007**, *46*, 4456.
- (14) Mannini, M.; Pineider, F.; Sainctavit, P.; Danieli, C.; Otero, E.; Sciancalepore, C.; Talarico, A. M.; Arrio, M. A.; Cornia, A.; Gatteschi, D.; Sessoli, R. *Nat. Mater.* **2009**, *8*, 194.
- (15) Loh, S.; von Bergmann, K.; Ternes, M.; Otte, A. F.; Lutz, C. P.; Heinrich, A. J. *Nat. Phys.* **2010**, *6*, 340.
- (16) Ishikawa, N.; Sugita, M.; Ishikawa, T.; Koshihara, S.; Kaizu, Y. *J. Am. Chem. Soc.* **2003**, *125*, 8694.
- (17) Ishikawa, N.; Sugita, M.; Ishikawa, T.; Koshihara, S.; Kaizu, Y. *J. Phys. Chem. B* **2004**, *108*, 11265.
- (18) AlDamen, M. A.; Clemente-Juan, J. M.; Coronado, E.; Martı́-Gastaldo, C.; Gaita-Ariño, A. *J. Am. Chem. Soc.* **2008**, *130*, 8874.
- (19) AlDamen, M. A.; Cardona-Serra, S.; Clemente-Juan, J. M.; Coronado, E.; Gaita-Ariño, A.; Martı́-Gastaldo, C.; Luis, F.; Montero, O. *Inorg. Chem.* **2009**, *48*, 3467.
- (20) Rinehart, J. D.; Long, J. R. *J. Am. Chem. Soc.* **2009**, *131*, 12558.
- (21) Edelstein, N. M.; Lander, G. H. In *The Chemistry of the Actinide and Transactinide elements*, 3rd ed.; Morss, L. R., Edelstein, N. M., Fuger, J., Katz, J. J., Eds.; Springer: Dordrecht, 2006; Vol. 4.
- (22) Orchard, A. F. *Magnetochemistry*; Oxford University Press: Oxford, 2003.
- (23) Wybourne, B. G. *Spectroscopic Properties of Rare Earths*; Wiley: New York, 1965.
- (24) Rinehart, J. D.; Harris, T. D.; Kozimor, S. A.; Bartlett, B. M.; Long, J. R. *Inorg. Chem.* **2009**, *48*, 3382.
- (25) Benelli, C.; Gatteschi, D. *Chem. Rev. (Washington, DC, U. S.)* **2002**, *102*, 2369.
- (26) Laplaza, C. E.; Cummins, C. C. *Science (Washington, DC, U. S.)* **1995**, *268*, 861.
- (27) Yandulov, D. V.; Schrock, R. R. *Science (Washington, DC, U. S.)* **2003**, *301*, 76.
- (28) Castro-Rodríguez, I.; Nakai, H.; Zakharov, L. N.; Rheingold, A. L.; Meyer, K. *Science (Washington, DC, U. S.)* **2004**, *305*, 1757.
- (29) Fryzuk, M. D. *Acc. Chem. Res.* **2009**, *42*, 127.
- (30) Knobloch, D. J.; Lobkovsky, E.; Chirik, P. J. *Nat. Chem.* **2010**, *2*, 30.
- (31) Jenkins, D. M.; Di Bilio, A. J.; Allen, M. J.; Betley, T. A.; Peters, J. C. *J. Am. Chem. Soc.* **2002**, *124*, 15336.
- (32) England, J.; Martinho, M.; Farquhar, E. R.; Frisch, J. R.; Bominaar, E. L.; Münck, E.; Que, L. *Angew. Chem., Int. Ed.* **2009**, *48*, 3622.
- (33) Brown, S. D.; Peters, J. C. *J. Am. Chem. Soc.* **2005**, *127*, 1913.
- (34) Diaconescu, P. L.; Arnold, P. L.; Baker, T. A.; Mindiola, D. J.; Cummins, C. C. *J. Am. Chem. Soc.* **2000**, *122*, 6108.
- (35) Mendiola, D. J.; Hillhouse, G. L. *J. Am. Chem. Soc.* **2001**, *123*, 4623.
- (36) Melenkivitz, R.; Mendiola, D. J.; Hillhouse, G. L. *J. Am. Chem. Soc.* **2002**, *124*, 3846.
- (37) Mendiola, D. J.; Hillhouse, G. L. *J. Am. Chem. Soc.* **2002**, *124*, 9976.
- (38) Andres, H.; Bominaar, E. L.; Smith, J. M.; Eckert, N. A.; Holland, P. L.; Münck, E. *J. Am. Chem. Soc.* **2002**, *124*, 3012.
- (39) Boca, R. *Coord. Chem. Rev.* **2004**, *248*, 757.
- (40) Merrill, W. A.; Stich, T. A.; Brynda, M.; Yeagle, G. J.; Fettinger, J. C.; De Hont, R.; Reiff, W. M.; Schulz, C. E.; Britt, R. D.; Power, P. P. *J. Am. Chem. Soc.* **2009**, *131*, 12693.
- (41) Reiff, W. M.; Schulz, C. E.; Whangbo, M.-H.; Seo, J. I.; Lee, Y. S.; Potratz, G. R.; Spicer, C. W.; Girolami, G. S. *J. Am. Chem. Soc.* **2008**, *131*, 404.
- (42) Reiff, W. M.; LaPointe, A. M.; Witten, E. H. *J. Am. Chem. Soc.* **2004**, *126*, 10206.
- (43) Popescu, C. V.; Mock, M. T.; Stoian, S. A.; Dougherty, W. G.; Yap, G. P. A.; Riordan, C. G. *Inorg. Chem.* **2009**, *48*, 8317.
- (44) Groves, J. T. *J. Inorg. Biochem.* **2006**, *100*, 434.
- (45) Bukowski, M. R.; Koehntop, K. D.; Stubna, A.; Bominaar, E. L.; Halfen, J. A.; Münck, E.; Nam, W.; Que, L. *Science (Washington, DC, U. S.)* **2005**, *310*, 1000.
- (46) de Oliveira, F. T.; Chanda, A.; Banerjee, D.; Shan, X. P.; Mondal, S.; Que, L.; Bominaar, E. L.; Münck, E.; Collins, T. J. *Science (Washington, DC, U. S.)* **2007**, *315*, 835.
- (47) Halfen, J. A.; Mahapatra, S.; Wilkinson, E. C.; Kaderli, S.; Young, V. G.; Que, L.; Zuberbühler, A. D.; Tolman, W. B. *Science (Washington, DC, U. S.)* **1996**, *271*, 1397.
- (48) Rohde, J. U.; In, J. H.; Lim, M. H.; Brennessel, W. W.; Bukowski, M. R.; Stubna, A.; Münck, E.; Nam, W.; Que, L. *Science (Washington, DC, U. S.)* **2003**, *299*, 1037.
- (49) Grapperhaus, C. A.; Mienert, B.; Bill, E.; Weyhermüller, T.; Wieghardt, K. *Inorg. Chem.* **2000**, *39*, 5306.
- (50) Berry, J. F.; Bill, E.; Bothe, E.; George, S. D.; Mienert, B.; Neese, F.; Wieghardt, K. *Science (Washington, DC, U. S.)* **2006**, *312*, 1937.
- (51) Holland, P. L. *Acc. Chem. Res.* **2008**, *41*, 905.
- (52) Bart, S. C.; Lobkovsky, E.; Bill, E.; Chirik, P. J. *J. Am. Chem. Soc.* **2006**, *128*, 5302.
- (53) Szazama, G. T.; Betley, T. A. *Inorg. Chem.* **2010**, *49*, 2512.
- (54) King, E. R.; Betley, T. A. *J. Am. Chem. Soc.* **2009**, *131*, 14374.
- (55) King, E. R.; Betley, T. A. *Inorg. Chem.* **2009**, *48*, 2361.
- (56) Thomas, C. M.; Mankad, N. P.; Peters, J. C. *J. Am. Chem. Soc.* **2006**, *128*, 4956.
- (57) Betley, T. A.; Peters, J. C. *J. Am. Chem. Soc.* **2004**, *126*, 6252.
- (58) Brown, S. D.; Betley, T. A.; Peters, J. C. *J. Am. Chem. Soc.* **2003**, *125*, 322.
- (59) Mukherjee, J.; Lucas, R. L.; Zart, M. K.; Powell, D. R.; Day, V. W.; Borovik, A. S. *Inorg. Chem.* **2008**, *47*, 5780.
- (60) Larsen, P. L.; Gupta, R.; Powell, D. R.; Borovik, A. S. *J. Am. Chem. Soc.* **2004**, *126*, 6522.
- (61) MacBeth, C. E.; Golombek, A. P.; Young, V. G.; Yang, C.; Kuczera, K.; Hendrich, M. P.; Borovik, A. S. *Science (Washington, DC, U. S.)* **2000**, *289*, 938.
- (62) Mock, M. T.; Popescu, C. V.; Yap, G. P. A.; Dougherty, W. G.; Riordan, C. G. *Inorg. Chem.* **2008**, *47*, 1889.
- (63) Scepaniak, J. J.; Young, J. A.; Bontchev, R. P.; Smith, J. M. *Angew. Chem., Int. Ed.* **2009**, *48*, 3158.
- (64) Scepaniak, J. J.; Fulton, M. D.; Bontchev, R. P.; Duesler, E. N.; Kirk, M. L.; Smith, J. M. *J. Am. Chem. Soc.* **2008**, *130*, 10515.
- (65) Nieto, I.; Ding, F.; Bontchev, R. P.; Wang, H. B.; Smith, J. M. *J. Am. Chem. Soc.* **2008**, *130*, 2716.

Scheme 1



pursued hybrid ligand scaffolds that combine attributes of heme and nonheme frameworks using trianionic tris(pyrrolyl- $\alpha$ -methyl)amines.<sup>69</sup> The addition of steric pickets to the  $[\text{tpa}]^{3-}$  platform serves to enforce an approximate three-fold symmetry while preventing dimerization. Furthermore, the wide range of potential ligand variants allows for facile tuning of the steric and electronic properties of the corresponding metal complexes. We recently disclosed the oxygen atom transfer chemistry of the iron complexes  $[(\text{tpa}^{\text{Ph}})\text{Fe}]^-$  and  $[(\text{tpa}^{\text{Mes}})\text{Fe}]^-$ , demonstrating intramolecular aromatic C–H hydroxylation by the former and activation of nitrous oxide and intermolecular hydrogen atom abstraction by the latter.<sup>69</sup> In addition to this novel reactivity, this ligand scaffold enforces a three-fold coordination geometry about a high-spin  $S = 2$  iron center. Importantly, the resulting electronic structure features three electrons in the  $1e$  orbital set, which leads to an unquenched orbital moment and thus the potential for strong magnetic anisotropy. Indeed, we recently demonstrated the efficacy of this strategy in our report of the magnetic properties of  $\text{K}[(\text{tpa}^{\text{Mes}})\text{Fe}]$ .<sup>70</sup> Magnetization measurements on this compound revealed the presence of immense uniaxial anisotropy, with an axial zero-field splitting parameter of  $D = -40 \text{ cm}^{-1}$ . Moreover, we demonstrated that this anisotropy leads to slow relaxation effects under the presence of a small applied dc field, with an effective relaxation barrier of  $U_{\text{eff}} = 42 \text{ cm}^{-1}$ , thereby providing the first example of a mononuclear transition metal complex exhibiting single-molecule magnet-like behavior.

The tunability of the  $[(\text{tpa}^{\text{R}})\text{Fe}]^-$  platform affords the opportunity to expand this concept to other mononuclear transition metal complexes. Herein, we report the design and synthesis of a homologous series of  $[(\text{tpa}^{\text{R}})\text{Fe}]^-$  complexes with various aryl and alkyl substituents, where R = *tert*-butyl (**1**), mesityl (**2**), 2,4,6-triisopropylphenyl (**3**), phenyl (**4**), and 2,6-difluorophenyl (**5**), as well as the structural, and magnetic properties of this novel series of trigonal pyramidal iron(II) complexes. Most importantly, we demonstrate the presence of strong uniaxial magnetic anisotropy in the complexes that engenders slow magnetic relaxation with barriers up to  $U_{\text{eff}} = 65 \text{ cm}^{-1}$  in the case of **1**. Moreover, our ability to vary the pendant substituents of the ligand across the series has enabled us to thoroughly examine the effect of factors such as ligand donor

strength and coordination geometry on governing magnetic anisotropy and slow magnetic relaxation.

## Results and Discussion

### Synthesis of $[\text{tpa}^{\text{R}}]$ Ligands and Their Iron(II) Complexes.

Inspired by the initial report of tris(pyrrolyl- $\alpha$ -methyl)amine ( $\text{H}_3\text{tpa}$ )<sup>71</sup> and a related indolyl system,<sup>72</sup> we sought to expand the steric and electronic properties of this platform into a family of tripodal pyrrolyl ligands. To this end, we prepared a series of 2-alkyl- and 2-arylpyrroles and subjected these precursors to Mannich reaction conditions adapted from the original synthesis of  $\text{H}_3\text{tpa}$ .<sup>71</sup> Whereas in our hands 2-alkylpyrroles containing pseudobenzyl protons (e.g., 2-methylpyrrole, 2-ethylpyrrole) gave ill-defined polymeric products under these reaction conditions, 2-*tert*-butylpyrrole (**11**) reacted smoothly to generate the new alkyl substituted variant  $\text{H}_3\text{tpa}^{t\text{-Bu}}$  (**6**) in good yield. In the interest of facilitating the development of this chemistry, we devised an improved synthesis of 2-*tert*-butylpyrrole that provides access to large quantities of this material (see Scheme 1). First, ethanolation of 2-(trichloroacetyl)pyrrole affords ethyl pyrrole-2-carboxylate (**16**). Friedel-Crafts alkylation of the pyrrole followed by saponification of the ethyl ester and decarboxylation yields analytically pure **11** on scales upward of 30 g without the need for chromatography. To further expand the utility of the  $[\text{tpa}^{\text{R}}]^{3-}$  ligand family, we prepared several 2-arylpyrroles (2-mesitylpyrrole (**12**), 2-(2,4,6-triisopropylphenyl)pyrrole (**13**) and 2-phenylpyrrole (**14**)) using a published procedure for the direct Pd-catalyzed arylation of sodium pyrrole<sup>73</sup> and also extended this methodology to the preparation of 2-(2,6-difluorophenyl)pyrrole (**15**) (see Scheme 1). All of these 2-arylpyrroles undergo triple Mannich condensation to provide the respective ligands in moderate to good yield. We have previously disclosed the syntheses of  $\text{H}_3\text{tpa}^{\text{Mes}}$  (**7**) and  $\text{H}_3\text{tpa}^{\text{Ph}}$  (**9**),<sup>69</sup> and the preparations of  $\text{H}_3\text{tpa}^{\text{Triip}}$  (**8**) and its molybdenum complexes have been described recently.<sup>74</sup> Vanadium complexes of  $[\text{tpa}^{\text{Mes}}]^{3-}$  have also been reported.<sup>75,76</sup>

Deprotonation of the  $\text{H}_3\text{tpa}^{\text{R}}$  proligands in situ followed by salt metathesis with  $\text{FeCl}_2$  in THF provides a general route to anionic iron(II) complexes, as isolated in  $[\text{M}(\text{sol})_n][(\text{tpa}^{\text{R}})\text{Fe}]$  ( $\text{M} = \text{Na}$ , R = *tert*-butyl (**1**), phenyl (**4**);  $\text{M} = \text{K}$ , R = mesityl (**2**), 2,4,6-triisopropylphenyl (**3**), 2,6-difluorophenyl (**5**)) (see

(66) Govindaswamy, N.; Quarless, D. A.; Koch, S. A. *J. Am. Chem. Soc.* **1995**, *117*, 8468.

(67) Nguyen, D. H.; Hsu, H. F.; Millar, M.; Koch, S. A.; Achim, C.; Bominaar, E. L.; Münck, E. *J. Am. Chem. Soc.* **1996**, *118*, 8963.

(68) Hwang, J.; Govindaswamy, K.; Koch, S. A. *Chem. Commun. (Cambridge, U. K.)* **1998**, 1667.

(69) Harman, W. H.; Chang, C. J. *J. Am. Chem. Soc.* **2007**, *129*, 15128.

(70) Freedman, D. E.; Harman, W. H.; Harris, T. D.; Long, G. J.; Chang, C. J.; Long, J. R. *J. Am. Chem. Soc.* **2010**, *132*, 1224.

(71) Shi, Y.; Cao, C.; Odom, A. L. *Inorg. Chem.* **2004**, *43*, 275.

(72) Tanski, J. M.; Parkin, G. *Inorg. Chem.* **2003**, *42*, 264.

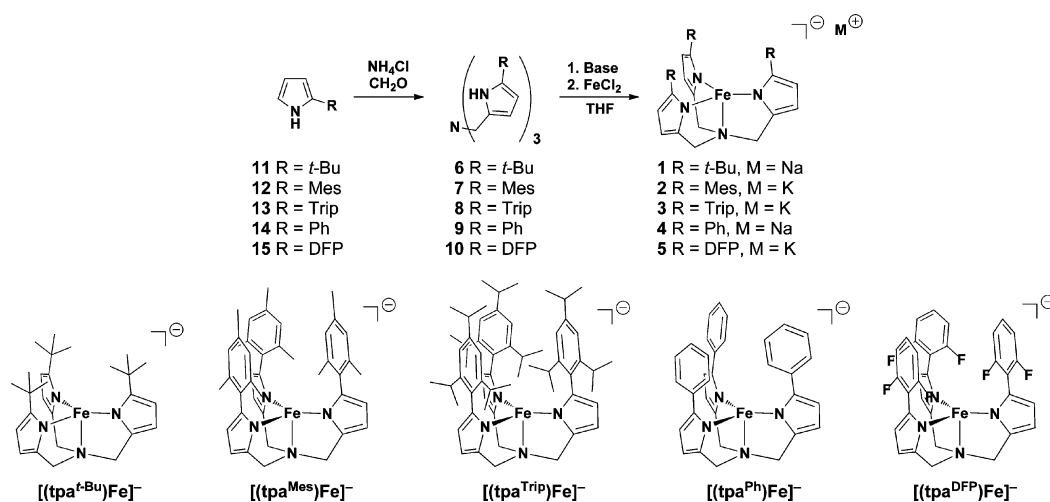
(73) Rieth, R. D.; Mankad, N. P.; Calimano, E.; Sadighi, J. P. *Org. Lett.* **2004**, *6*, 3981.

(74) Wampler, K. M.; Schrock, R. R. *Inorg. Chem.* **2007**, *46*, 8463.

(75) Betley, T. A.; Wu, Q.; Van Voorhis, T.; Nocera, D. G. *Inorg. Chem.* **2008**, *47*, 1849.

(76) Betley, T. A.; Surendranath, Y.; Childress, M. V.; Alliger, G. E.; Fu, R.; Cummins, C. C.; Nocera, D. G. *Philos. Trans. R. Soc. London, Ser. B.* **2008**, *363*, 1293.

## Scheme 2



Scheme 2). Counterion choice is dictated primarily by the solubility and crystallinity of the product. Potassium hydride proved to be a suitable base for the syntheses of **2**, **3**, and **5**. Sodium hydride was employed in the synthesis of **4** whereas NaN(SiMe<sub>3</sub>)<sub>2</sub> was used to furnish the desired sodium salt **1**.

**Solid-State Structures.** Compounds **1–5** crystallize readily as THF or DME solvates. Single crystal X-ray diffraction measurements reveal four-coordinate, trigonal pyramidal iron centers for each complex, as depicted in Figure 1. Although **3** crystallizes readily and in high yield, issues with twinning and disorder have thus far impeded our efforts to obtain satisfactory solutions to data collected on these crystals. Relevant bond lengths and angles for **1**, **2**, **4**, and **5** are listed in Table 1. The Fe–N<sub>pyrrole</sub> distances range from 2.008(3) Å to 2.042(3) Å for the series, consistent with anionic nitrogen ligation of high-spin iron(II). The longer axial Fe–N<sub>amine</sub> distances vary over a slightly larger range from 2.144(1) Å to 2.196(2) Å.

The *tert*-butyl derivative **1** crystallizes in the cubic space group *P*<sub>2</sub><sub>1</sub><sub>3</sub> and is unique among iron(II) complexes **1–5** in that it possesses crystallographically imposed three-fold symmetry at the iron center. The iron centers in **2**, **4**, and **5** exhibit slight deviations from three-fold symmetry. The most pronounced structural distortion is observed for **2**, in which a mesityl *o*-methyl group (C42) is rotated toward the iron center. The Fe–N<sub>pyrrole</sub> bond directly opposite the iron-methyl close contact is anomalously short at 2.008(3) Å.

**Static Magnetic Properties.** With structural data for this family of trigonal pyramidal nonheme iron(II) complexes in hand, we turned our attention to more comprehensively interrogating their magnetic properties. Dc magnetic susceptibility measurements

**Table 1.** Summary of Bond Lengths (Å) and Angles (deg) for the X-ray Structures of **1**, **2**, **4**, and **5**

	1	2	4	5
Fe1–N1	2.144(1)	2.172(2)	2.161(2)	2.196(2)
Fe1–N2	2.031(1)	2.008(3)	2.016(1)	2.036(2)
Fe1–N3		2.041(2)	2.013(2)	2.042(3)
Fe1–N4		2.024(3)	2.019(2)	2.038(3)
Fe1–N <sub>pyrrole</sub>		2.024	2.016	2.039
N2–Fe1–N3	118.35(6)	117.36(9)	115.56(6)	121.6(1)
N3–Fe1–N4		122.39(9)	120.22(7)	115.8(1)
N4–Fe1–N2		115.3(1)	120.27(6)	116.6(1)
Fe1–(N2,N3,N4)	0.263	0.262	0.233	0.290
Fe–Fe	9.482	10.651	8.927	9.277

at 300 K give values of  $\chi_{MT} = 3.55, 3.32,^{70} 3.68, 3.66,$  and  $3.44 \text{ cm}^3\text{mol/K}$  for compounds **1–5**, respectively (see Supporting Information Figures S1, S4, S9, and S14), confirming the presence of a high-spin electron configuration and an *S* = 2 spin ground state for each compound. Notably, each set of  $\chi_{MT}$  data displays a downturn at low temperature, suggesting the presence of significant zero-field splitting. To investigate this possibility, we collected low-temperature magnetization data at various applied dc fields for the compounds. The resulting plot of reduced magnetization for **1**, depicted in Figure 2, reveals a series of nonsuperimposable isofield curves that fall dramatically short of reaching the magnetization saturation of  $4.0 \mu_B$  expected for an *S* = 2 ground state with *g* = 2.0, confirming the presence of strong magnetic

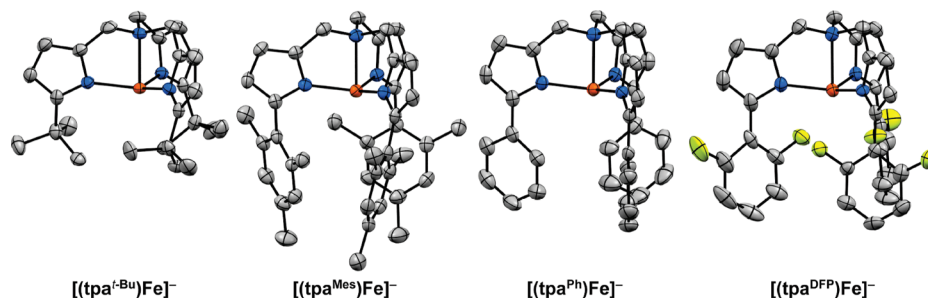


**Figure 1.** Thermal ellipsoid plots of the trigonal pyramidal complexes in **1**, **2**, **4**, and **5**. Ellipsoids are shown at the 50% probability level. Orange, blue, yellow, and gray ellipsoids represent Fe, N, F, and C atoms, respectively. Hydrogen atoms have been omitted for clarity.

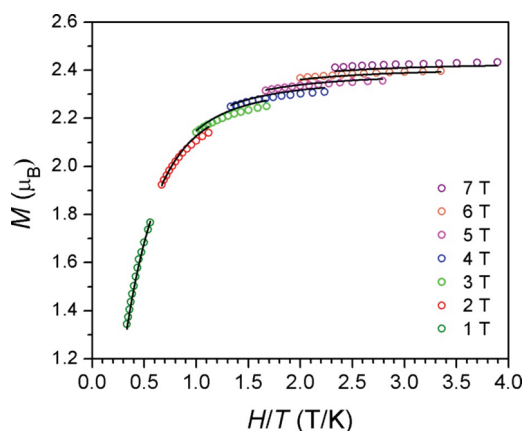


**Figure 2.** Low-temperature magnetization data for **1** collected under various applied dc fields. The black lines represent fits to the data.

anisotropy. To quantify this effect, the data were modeled according to the following spin Hamiltonian:

$$\hat{H} = D\hat{S}_z^2 + E(\hat{S}_x^2 - \hat{S}_y^2) + g_{\text{iso}}\mu_B\mathbf{S}\cdot\mathbf{H} \quad (1)$$

where  $S$  is the spin ground state,  $D$  is the axial zero-field splitting parameter,  $E$  is the transverse zero-field splitting parameter,  $g_{\text{iso}}$  is the average  $g$ -factor,  $\mu_B$  is the Bohr magneton, and  $H$  is magnetic field. Here, application of a Hamiltonian considering second-order anisotropy originating from zero-field splitting faces some limitation, as very strong first-order anisotropy can sometimes be better modeled by directly considering spin-orbit coupling of the ground state. Indeed, a recent report treated the magnetization data for compound **2** in such a fashion, employing a ligand field Hamiltonian that assumes the anisotropy arises from orbital degeneracy of the iron(II) ion.<sup>77</sup> However, this approach assumes rigorous three-fold site symmetry at the iron(II) center in order to preserve the orbital degeneracy. This is clearly not a valid assumption in the case of compounds **2–5**, as the crystal structure reveals that each complex undergoes a significant Jahn-Teller distortion to break the three-fold symmetry. Moreover, despite its apparent crystallographic  $C_3$  axis at 128 K, compound **1** may undergo a similar Jahn-Teller distortion at lower temperature or exhibit a more subtle distortion that is obscured by the thermal motion and three-fold symmetry of the crystal lattice. Thus, the zero-field splitting model likely provides a better physical description of the magnetic behavior of these complexes than does a model that assumes perfect three-fold symmetry and true orbital degeneracy.

Fits to the data obtained using ANISOFIT 2.0<sup>78</sup> give axial and transverse zero-field splitting parameters of  $D = -48 \text{ cm}^{-1}$  and  $|E| \leq 0.4 \text{ cm}^{-1}$ , respectively, with  $g = 2.28$ . The presence of such strong axial anisotropy arises from the quenched orbital angular momentum associated with a  $1e^32e^2a_1^1$  electronic configuration.<sup>70</sup> In contrast to this strong uniaxial anisotropy, the value of  $E$  is small, over 2 orders of magnitude smaller than  $D$ . The presence of such a large  $|D/E|$  ratio likely arises due to the crystallographic three-fold symmetry at the iron(II) center, which minimizes the magnetic anisotropy within the

**Table 2.** Summary of Magnetic Parameters for **1–5**<sup>a</sup>

	1	2	3	4	5
$g$	2.3(1) <sup>b</sup>	2.2(1)	2.4(1)	2.4(1)	2.0(1)
$D$	-48	-44(4)	-30(2)	-26(2)	-6.2
$ E _{\text{max}}$	0.4	6	4	5	0.1
$U_{\text{eff}}$	65	42	—	25	—

<sup>a</sup>All energies are given in  $\text{cm}^{-1}$ . <sup>b</sup>See Experimental Section for explanation of uncertainties.

trigonal plane of the molecule. Importantly, this large negative value of  $D$ , in conjunction with the high-spin  $S = 2$  ground state, demonstrates the potential of this type of mononuclear transition metal complex to exhibit slow magnetic relaxation. Indeed, a compound exhibiting these parameters could display a maximal thermal relaxation barrier of  $U = S^2|D| = 192 \text{ cm}^{-1}$ , which would be by far the record barrier for a transition metal system.<sup>5</sup>

Zero-field splitting parameters extracted from fits to reduced magnetization data collected for **1–5** are enumerated in Table 2 (see Supporting Information Figures S5, S10, and S15). For all of the compounds, the best fits to the data give negative values of  $D$ , indicative of a uniaxial anisotropy and thus the possibility of slow magnetic relaxation. The series of  $D$  values ranges from  $D = -48 \text{ cm}^{-1}$  for **1** to  $D = -6.2 \text{ cm}^{-1}$  in the case of **5**. Inspection of the trend across the series reveals a dependence of the magnitude of  $D$  on Lewis base strength, where the magnitude of  $D$  rises with increasing basicity of the ligand. This observation suggests that the magnitude of axial anisotropy may be related to the energy separation between the  $1e$  ( $d_{xz}$  and  $d_{yz}$ ) and  $2e$  ( $d_{xy}$  and  $d_{x^2-y^2}$ ) orbitals, as the energy of the  $2e$  orbitals will increase with the  $\sigma$ -donating ability of the ligand. Taken together, these data establish that the trigonal pyramidal  $[(\text{tpa}^R)\text{Fe}]^-$  system offers a general platform for obtaining large uniaxial zero-field splitting.

**Dynamic Magnetic Properties.** To investigate the potential for slow magnetic relaxation in this homologous series of high-spin iron(II) compounds, we collected variable-frequency ac susceptibility data at multiple temperatures. In the absence of an applied dc field, no  $\chi_M''$  signals were observed at frequencies up to 1500 Hz and temperatures down to 1.8 K. This result is somewhat unexpected, given the large uniaxial anisotropy and  $S = 2$  spin ground states determined for the compounds through static magnetic measurements. One explanation for the absence of  $\chi_M''$  signals is that quantum tunneling of the magnetization through the thermal relaxation barrier dominates other relaxation pathways in the absence of an applied dc field. Such tunneling processes may arise due to the presence of transverse magnetic anisotropy in the compounds. For a molecule exhibiting rigorously axial anisotropy, the wave functions corresponding to each  $\pm M_S$  pair do not overlap with one another, such that no mixing can occur between the two.<sup>3,79</sup> In this case, quantum tunneling is a forbidden process. If a transverse component to the magnetic anisotropy is introduced, however, mixing between these wave functions occurs. This mixing then enables the magnetization of the  $+M_S$  level to tunnel through the anisotropy barrier to the  $-M_S$  level, such that the overall relaxation time is fast. As has been observed for a number of previously reported compounds, tunneling effects can drastically reduce the relaxation time of a single-molecule magnet.<sup>20,79–83</sup> Indeed, the

(77) Palii, A. V.; Clemente-Juan, J. M.; Coronado, E.; Klokishner, S. I.; Ostrovsky, S. M.; Reu, O. S. *Inorg. Chem.* **2010**, *49*, 8073.

(78) Shores, M. P.; Sokol, J. J.; Long, J. R. *J. Am. Chem. Soc.* **2002**, *124*, 2279.

(79) Gatteschi, D.; Sessoli, R. *Angew. Chem., Int. Ed.* **2003**, *42*, 268.

(80) Friedman, J. R.; Sarachik, M. P.; Tejada, J.; Ziolo, R. *Phys. Rev. Lett.* **1996**, *76*, 3830.

smaller ratios of  $|D/E|$  observed for **2–5** support the hypothesis that quantum tunneling provides a facile relaxation pathway for the compounds. Somewhat surprisingly, despite exhibiting crystallographic three-fold symmetry and a miniscule value of  $E$ , compound **1** relaxes rapidly on the timescale of the ac susceptibility experiment under zero applied dc field. In addition to slight deviations from ideal three-fold symmetry at the iron(II) center in **1** that may be undetectable in the crystal structure due to thermal motion of the nitrogen atoms at 128 K, this rapid relaxation in the absence of an applied field is also likely the result of tunneling. In this context, the tunneling probability is known to increase with decreasing  $M_S$ <sup>79,84</sup> and this monoiron system has a relatively small spin ground state of  $S = 2$ . Finally, as the magnetic measurements were performed on microcrystalline solids, fast relaxation in zero-field may be facilitated by spin-spin interactions between neighboring iron(II) ions. This hypothesis is consistent with the Mössbauer spectra obtained for these systems, which, as discussed below, reveal a temperature independence of the relaxation time below 10 K.

If quantum tunneling and/or spin-spin relaxation effects are in fact responsible for shortcutting of the thermal relaxation barriers in the iron(II) complexes, then application of a dc field during the ac measurement should act to split the energies of the  $\pm M_S$  pairs, thereby eliminating tunneling as a facile relaxation pathway and slowing down the relaxation dynamics. Indeed, just such an experiment leads to slow relaxation effects for all compounds with the exception of **5**. For instance, data collected for **1** under a 1500 Oe dc field reveal a set of temperature-dependent peaks in the plot of  $\chi_M''$  vs  $\nu$  (see Figure 3, bottom). In order to extract relaxation times from these peaks, we constructed Cole–Cole plots from data collected in the temperature range 1.8–6.8 K and fit them to a generalized Debye model.<sup>85–87</sup> For a single-molecule magnet, the relaxation time ( $\tau$ ) follows a thermally activated relaxation process where  $\tau$  increases exponentially with decreasing temperature. Accordingly, the corresponding plot of  $\ln(\tau)$  vs  $1/T$  should feature a linear region, with the slope of that line giving the relaxation energy barrier. Indeed, the Arrhenius plot constructed for **1** (see Figure 3, top) features a linear region at high temperature, with a least-squares fit giving  $U_{\text{eff}} = 65 \text{ cm}^{-1}$  and  $\tau_0 = 6.7 \times 10^{-11} \text{ s}$ . The value of  $\tau_0$  provides a quantitative measure of the attempt time of relaxation from the thermal phonon bath, and the value obtained here is comparable to those found in single-molecule magnets.<sup>1–5</sup> In addition, this value of  $\tau_0$  eliminates the possibility that phonon bottleneck effects lead to the observed slow relaxation.<sup>88</sup>

The large temperature range over which slow relaxation is observed for **1** at 1500 Oe provides a comprehensive map of the relaxation processes occurring within the molecule. At this

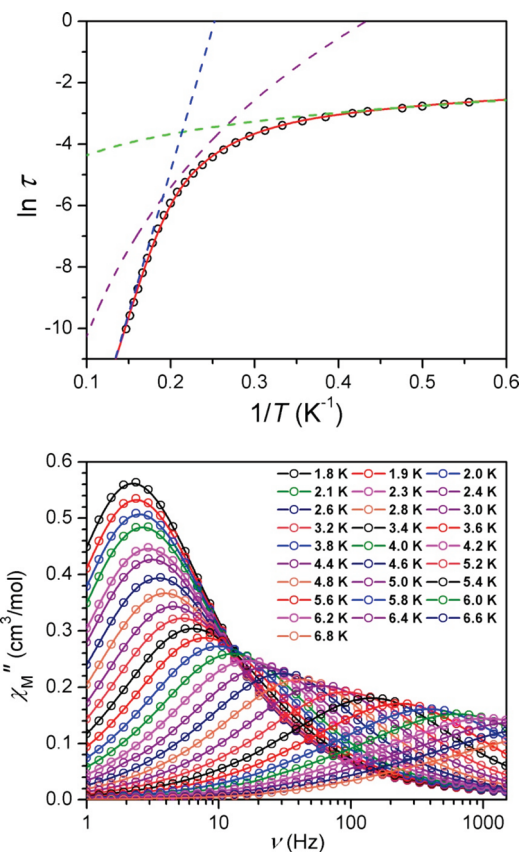


**Figure 3.** Bottom: Variable-frequency out-of-phase ac susceptibility data for **1**, collected under a 1500 Oe dc field at various temperatures. The solid lines are guides for the eye. Top: Arrhenius plot constructed from data obtained under a dc field of 1500 Oe. The dashed lines represent data fits to an Orbach (blue), Raman (purple), and direct (green) process. The solid red line represents a data fit to the three processes simultaneously.

applied dc field, the relaxation is dominated by spin-lattice interactions.<sup>89,90</sup> For instance, at high temperature, the relaxation time exhibits a clear Arrhenius dependence, with  $\ln(\tau)$  increasing linearly with  $1/T$  (see Figure 3, upper, dashed blue line). This region is likely dominated by an Orbach relaxation process, sometimes referred to as thermally assisted quantum tunneling of the magnetization. Here, a spin associated with the  $M_S = +2$  level absorbs a phonon and is excited to the  $M_S = +1$  level. Then, the spin tunnels from the  $M_S = +1$  to  $M_S = -1$  level and subsequently relaxes to the  $M_S = -2$  level. Note, though, that this process cannot be the sole relaxation pathway operating at these temperatures, because such a scenario would give a relaxation barrier of  $U_{\text{eff}} = 144 \text{ cm}^{-1}$ , the energy associated with climbing from the  $M_S = +2$  to  $M_S = +1$  level. At low temperature,  $\ln(\tau)$  also exhibits a linear dependence on  $1/T$ , albeit with a slope of nearly zero (see Figure 3, upper, dashed green line). This region is likely dominated by ground-state tunneling via a direct phonon-based relaxation process, as insufficient thermal energy is available for a spin to relax via a thermally assisted mechanism. In the case of **1**, this process corresponds to tunneling from the  $M_S = +2$  to  $M_S = -2$  level. Since the  $\ln(\tau)$  data do not show a clear transition between a high temperature Orbach region and a low temperature direct process region, a Raman relaxation mechanism was considered in order

(81) Thomas, L.; Lionti, F.; Ballou, R.; Gatteschi, D.; Sessoli, R.; Barbara, B. *Nature* **1996**, *383*, 145.

(82) Sangregorio, C.; Ohm, T.; Paulsen, C.; Sessoli, R.; Gatteschi, D. *Phys. Rev. Lett.* **1997**, *78*, 4646.

(83) Lin, P. H.; Burchell, T. J.; Clérac, R.; Murugesu, M. *Angew. Chem., Int. Ed.* **2008**, *47*, 8848.

(84) Chudnovsky, E. M.; Tejada, J. *Macroscopic Tunneling of the Magnetic Moment*; Cambridge University Press: Cambridge, UK, 1998.

(85) Cole, K. S.; Cole, R. H. *J. Chem. Phys.* **1941**, *9*, 341.

(86) Böttcher, C. J. F. *Theory of Electric Polarisation*; Elsevier: New York, 1952.

(87) Aubin, S. M. J.; Sun, Z. M.; Pardi, L.; Krzystek, J.; Foltng, K.; Brunel, L. C.; Rheingold, A. L.; Christou, G.; Hendrickson, D. N. *Inorg. Chem.* **1999**, *38*, 5329.

(88) Schenker, R.; Leuenberger, M. N.; Chaboussant, G.; Loss, D.; Güdel, H. U. *Phys. Rev. B: Condens. Matter Mater. Phys.* **2005**, *72*, 184403.

(89) Abragam, A.; Bleaney, B. *Electron Paramagnetic Resonance of Transition Ions*; Clarendon Press: Oxford, U. K., 1970.

(90) Carlin, R. L. *Magnetochemistry*; Springer-Verlag: Berlin, 1986.

to model the intermediate data (Figure 3, upper, dashed purple line). In this process, the relaxation time scales with temperature, intermediate between the exponential (Orbach) and direct dependences on  $1/T$ . The crossover between Arrhenius behavior and direct tunneling through an intermediate Raman process is prevalent among mononuclear and weakly exchange-coupled multinuclear single-molecule magnets, yet previous fitting of variable-temperature relaxation time data has included only the Orbach region.<sup>20,70,83</sup> To our knowledge, these data mark the first time that the temperature dependence of the relaxation time in a molecule has been fit to a non-Orbach mechanism (see Figure 3, upper, solid red line).

We conducted similar ac susceptibility measurements on the other  $[\text{tpa}^R\text{Fe}]^-$  compounds (see Supporting Information Figures S6–S8 and S11–S13). Arrhenius fits to relaxation times extracted from Cole-Cole plots give relaxation barriers of  $U_{\text{eff}} = 42 \text{ cm}^{-1}$  for **2** and  $25 \text{ cm}^{-1}$  for **4**. In the case of **3**, we observe a temperature- and frequency-dependent  $\chi_M''$  signal; however, the corresponding relaxation times are not indicative of thermally activated behavior. As such, no thermal relaxation barrier could be obtained in the measured temperature range. With the exception of **3**, the magnitude of  $U_{\text{eff}}$  increases with increasing value of  $D$ . The absence of slow relaxation observed for **5** is likely a direct consequence of the low  $D$  value of the compound.

**Mössbauer Spectroscopy.** In view of the fast relaxation processes that dominate the magnetization dynamics of the iron(II) complexes under zero field at low temperature, we carried out zero-field Mössbauer spectroscopy measurements to probe these processes on a much faster time scale (ca. 0.01  $\mu\text{s}$ ). For these studies, we focused our attention on compounds **1**, **2**, and **4** in order to compare and contrast alkyl versus aryl substitution on the ancillary tpa framework.<sup>91</sup> Selected Mössbauer spectra of **1** obtained at various temperatures are shown in the left panel of Figure 4. At 220, 180, and 120 K, the spectra consist of a paramagnetic quadrupole doublet with an isomer shift characteristic of iron(II) accounting for the majority of the sample. A minor doublet is assigned to a small amount of an iron(III)-containing impurity. The isomer shift of  $\delta = 0.85 \text{ mm/s}$  observed for **1** at 4.2 K is consistent with a high-spin iron(II) ion in a four-coordinate environment.<sup>92</sup> Notably, the quadrupole splitting ( $\Delta E_Q$ ) observed for **1** is very small and positive. This splitting arises from two contributions to the electric field gradient, the lattice ( $q_{\text{lat}}$ ) and valence ( $q_{\text{val}}$ ) components. The crystallographic three-fold symmetry of the iron complex in **1** generates a d-orbital manifold qualitatively similar to that of a tetrahedron, a geometry for which  $q_{\text{val}}$  is expected to be essentially zero. In addition, the cubic symmetry of the lattice in which **1** crystallizes likewise contributes to a highly uniform electric field gradient. The presence of a simple quadrupole doublet above 120 K indicates that the magnetic relaxation of **1** is fast relative to the Larmor precession time of the iron-57 nuclear magnetic moment (ca. 0.01  $\mu\text{s}$ ). Specifically, simulations indicate that, for the hyperfine parameters observed for **1** at these temperatures, the relaxation time must be less than 0.005  $\mu\text{s}$ .

As the temperature is decreased below 120 K, the spectral profile of **1** broadens from a doublet to an asymmetric absorption, ultimately reaching a broad complex shape at 4.2 K. The broadening of the spectra with decreasing temperature results from the onset of slow magnetic relaxation down to 4.2 K, in accordance with the results of ac susceptibility experiments. In order to quantify this effect, the spectra were fit according to the Dattagupta and Blume formalism (see Supporting Information for a detailed description of this fitting).<sup>93</sup> Here, the relaxation of the magnetic hyperfine field,  $H_{\text{eff}}$ , of the iron(II) center is best modeled as occurring in  $120^\circ$  steps perpendicular to the  $C_3$  axis of the molecule, along each Fe–N<sub>pyrrole</sub> bond. Notably, the fit to the data reveals a hyperfine field of  $H_{\text{eff}} = 5.31(6) \text{ T}$ , a much smaller value than is commonly observed for high-spin iron(II) complexes. This reduced value is likely a result of the large unquenched orbital angular momentum in **1**, consistent with the strong magnetic anisotropy determined through magnetization experiments. Indeed, a similar phenomenon has been observed in the mixed-valence oxalates (PPh<sub>4</sub>)[Fe<sub>2</sub>(ox)<sub>3</sub>] and (NBu<sub>4</sub>)[Fe<sub>2</sub>(ox)<sub>3</sub>].<sup>94</sup>

An Arrhenius plot of the relaxation times obtained from fitting the spectra for **1** is shown in Figure 5. Between 4.2 and 10 K, the relaxation time is essentially independent of temperature, suggesting that the relaxation process is governed by spin–spin relaxation and/or quantum tunneling under zero applied magnetic field. In contrast, between 10 and 80 K, the relaxation time demonstrates a strong temperature dependence, with a linear least-squares fit providing a relaxation barrier of  $U_{\text{eff}} = 9.8(5) \text{ cm}^{-1}$ . This result indicates that a thermally activated Orbach mechanism dominates the relaxation process above 10 K. Interestingly, while a similar relaxation mechanism was observed from ac susceptibility experiments, the relaxation barrier of  $U_{\text{eff}} = 9.8(5) \text{ cm}^{-1}$  obtained from Mössbauer spectral fits is much smaller than that of  $U_{\text{eff}} = 65 \text{ cm}^{-1}$  from magnetic measurements. This difference may arise in large part due to the presence of fast relaxation processes in zero field, such as spin–spin relaxation and quantum tunneling, that serve to shortcut the thermal relaxation processes. Nevertheless, these data confirm that slow magnetic relaxation does indeed occur for **1** in the absence of an applied magnetic field. Finally, it should be noted that an adequate fit of the 4.2 and 10 K spectra of **1** requires a second component of 13(1)% area with a faster relaxation time of ca. 0.002  $\mu\text{s}$ . This observation may indicate that a small portion of the sample has a slightly different coordination environment or a slightly different interaction with the lattice and hence a differing extent of spin–lattice coupling.

Mössbauer spectra collected for compound **4** at selected temperatures are shown in the right panel of Figure 4. Here, the isomer shift of  $\delta = 0.858(2) \text{ mm/s}$  and small negative quadrupole splitting at 4.2 K confirm the presence of high-spin iron(II) in a high-symmetry four-coordinate environment. In the temperature range 80–220 K, the spectra consist of a narrow doublet, indicative of fast magnetic relaxation. As in the case of **1**, simulations indicate that the hyperfine field of **4** must be relaxing faster than 0.005  $\mu\text{s}$  in this temperature range. As the temperature is lowered, the doublet broadens to a complex peak similar to that observed for **1** below 10 K. In contrast to that observed for **1**, however, the line shape continues to evolve until

(91) The following discussion will emphasize the different relaxation times observed for **1** and **4**. The details of the relaxation model used to fit the spectra and an expanded discussion of the hyperfine parameters are given in the Supporting Information; the temperature dependence of the spectral parameters is shown in Figure S17 and the spectral fit parameters are given in Tables S1–S3.

(92) Reiff, W. M.; Long, G. J. In *Mössbauer Spectroscopy Applied to Inorganic Chemistry*; Long, G. J., Ed.; Plenum Press: New York, 1984; Vol. 1, p 245.

(93) Dattagupta, S.; Blume, M. *Phys. Rev. B: Condens. Matter Mater. Phys.* **1974**, *10*, 4540.

(94) Carling, S. G.; Visser, D.; Hautot, D.; Watts, I. D.; Day, P.; Enslin, J.; Gütllich, P.; Long, G. J.; Grandjean, F. *Phys. Rev. B: Condens. Matter Mater. Phys.* **2002**, *66*, 104407.

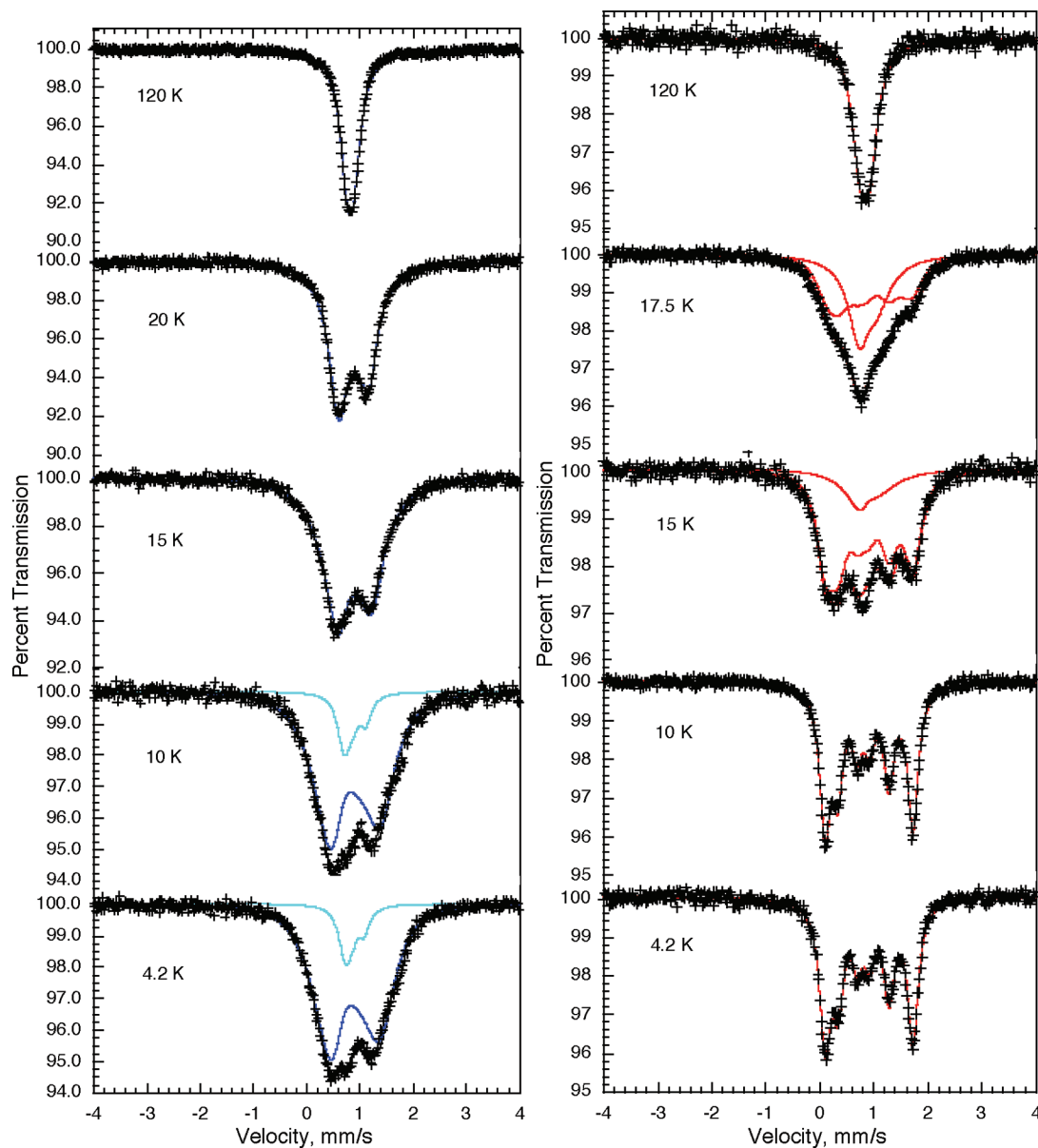


**Figure 4.** Variable temperature Mössbauer spectra of **1** and **4**.

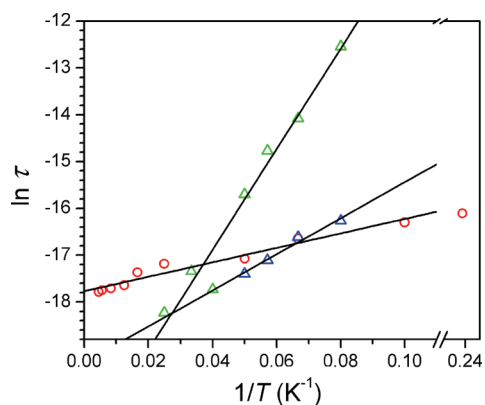


**Figure 5.** Arrhenius plot of relaxation time, as obtained from Mössbauer measurements, for **1** (red circles) and two relaxation processes for **4** (green and blue triangles). Solid black lines represent linear least-squares fits to the data.

finally forming a well-resolved sextet below 10 K. The observation of this sextet demonstrates the presence of magnetic

relaxation even slower than that observed in **1**. To further investigate this phenomenon, the spectra were modeled similarly to those for complex **1** (see Supporting Information). Here, however, acceptable fits of the relaxation spectra obtained in the temperature range 12.5–20 K required two spectral components with different relaxation times (see Figure 4). The need for two relaxation times may indicate the presence of two distinct or a small distribution of iron(II) coordination environments in **4**, perhaps as a result of partial DME desolvation. Similar to that observed for **1**, the fits reveal an unusually small hyperfine field of  $H = 4.95(1)$  T, indicative of strong magnetic anisotropy. The corresponding Arrhenius plots of relaxation time for the two modes both show a thermally activated behavior (see Figure 5), demonstrating that the hyperfine field of the iron(II) center is relaxing via an Orbach process in this temperature range. Least-squares fits to the two data sets give relaxation barriers of  $26(2)$  and  $75(4)$   $\text{cm}^{-1}$ . Remarkably, the barrier of  $26(2)$   $\text{cm}^{-1}$  is in accordance with that obtained from ac susceptibility data obtained for compound **4** at much lower

temperatures under a dc field of 1500 Oe. In contrast, the second process, corresponding to a barrier of  $75(4) \text{ cm}^{-1}$ , was undetected in our ac measurements with or without an applied dc field. Note that the magnitude of this barrier corresponds exactly to the energy separation between the  $|M_S| = 2$  and  $|M_S| = 1$  levels, considering the axial zero-field splitting parameter of  $D = -26(2) \text{ cm}^{-1}$  obtained from fitting magnetization data and the expression  $\Delta E = |(M_{S_2})^2 D| - |(M_{S_1})^2 D|$ . This barrier may thus represent a pure Orbach mechanism that is quenched at low temperatures or upon application of a dc field. Owing to the large separation between the  $M_S = \pm 2$  and  $\pm 1$  levels, there is no substantial population of the  $M_S = \pm 1$  levels up to ca. 40 K, a temperature at which the relative Boltzmann population of the  $M_S = \pm 1$  levels is 6%. Hence, a single sharp sextet is observed for **4** at 4.2 K.

In contrast to the relaxation observed in the Mössbauer spectra of **1** and **4**, the spectra of **2** obtained between 4.2 and 270 K consist of a paramagnetic doublet with a splitting that decreases from  $\Delta E_Q = 1.30 \text{ mm/s}$  at 4.2 K to  $\Delta E_Q = 0.67 \text{ mm/s}$  at 270 K (see Supporting Information Figure S16). This splitting is much larger than that observed for **1** and **4**, and this difference could result from the more distorted coordination environment for the iron(II) center. The absence of slow magnetic relaxation in **2**, in stark contrast to the dynamic behavior observed in ac magnetic susceptibility experiments, may stem from desolvation in the compound, which loses two molecules of DME when removed from its mother liquor. Such desolvation leads to a loss of crystallinity, which likely decreases the average Fe...Fe distance, thereby facilitating fast magnetic relaxation through spin-spin interactions.

#### High-Field Electron Paramagnetic Resonance Spectroscopy.

Finally, in order to probe directly the energy separation between the  $M_S$  levels and thus the zero-field splitting of the iron(II) complexes, we carried out high-field EPR experiments on polycrystalline samples of **1–5**. Variable-field spectra collected for the difluorophenyl-substituted compound **5** at 30 K and various frequencies (see Figure 6) reveal the presence of up to two transitions at each frequency, excluding the omnipresent peak at  $g \approx 2$  that likely stems from a small impurity. The low-field peak corresponds to the forbidden  $M_S = 2 \rightarrow M_S = -2$  transition, whereas the high-field peak corresponds to the allowed  $M_S = -2 \rightarrow M_S = -1$  transition. We note that the  $\Delta M_S = 4$  transition in iron(II) complexes may sometimes be observed even in X-band EPR spectra owing to the fact that the  $M_S = +2$  and  $-2$  levels are split only by approximately  $3E^2/D$ , while splittings between other  $M_S$  levels are of the order of  $E$  or  $D$ . To quantify the energies of the observed transitions, we used the frequency dependence of the peaks to construct a plot of resonance field vs frequency (see Figure 7). The data were then fit according to the following spin Hamiltonian:

$$\hat{H} = \mu_B \mathbf{H} \cdot \mathbf{g} \cdot \mathbf{S} + D(\hat{S}_z^2 - S(S+1)/3) + E(\hat{S}_x^2 - \hat{S}_y^2) \quad (2)$$

The best fits to the data provide zero-field splitting parameters of  $|D| = 4.397(9) \text{ cm}^{-1}$  and  $|E| = 0.574(9) \text{ cm}^{-1}$ , with  $g = 2.20$ . These parameters are in reasonable agreement with those of  $D = -6.2 \text{ cm}^{-1}$  and  $|E| = 0.1 \text{ cm}^{-1}$  obtained from fits to reduced magnetization data. In order to ascertain the sign of  $D$  for compound **5**, spectra were collected at 224 GHz at various temperatures. As shown in Supporting Information Figure S18, the intensity of the  $\Delta M_S = 4$  transition dramatically increases as the temperature is decreased. In contrast, the intensity of the allowed  $\Delta M_S = 1$  transition increases as the temperature is

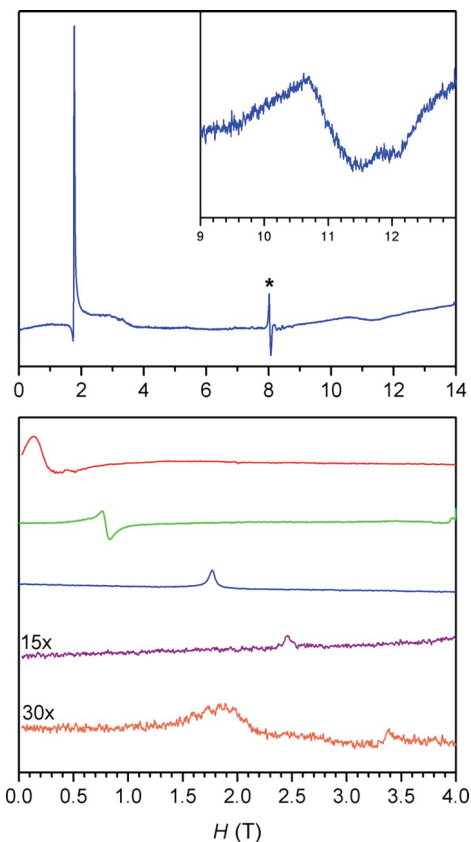


**Figure 6.** Top: Variable-field EPR spectrum for **5** collected at 10 K and 224 GHz. The asterisk denotes an impurity positioned at  $g \approx 2$ . Inset: Expanded view of the high-field portion of the spectrum. Bottom: Spectra for **5** collected at 30 K and frequencies of 56 (red), 112 (green), 224 (blue), 305 (purple), and 416 (magenta) GHz.

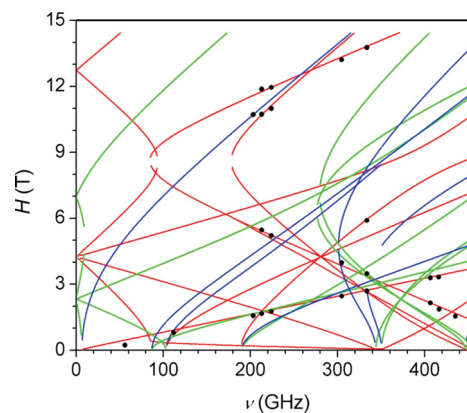


**Figure 7.** Resonant field vs frequency plot for **5**, constructed from data obtained at 30 K. Solid lines represent fits to the data, with x (red), y (blue), and z (green) turning points, to give  $|D| = 4.397(9) \text{ cm}^{-1}$ ,  $|E| = 0.574(9) \text{ cm}^{-1}$  and  $g = 2.20$ .

increased. These observations indicate the presence of an  $M_S$  manifold in which the largest values of  $M_S$  are lowest in energy, corresponding to a negative  $D$  value. This uniaxial anisotropy is consistent with the results from magnetization measurements.

High-field EPR spectra obtained for complexes **1–4** display the forbidden  $\Delta M_S = 4$  transition, but we observe no well-resolved peaks corresponding to allowed transitions at magnetic fields up to 14 T and frequencies up to 600 GHz. Since a transition corresponding to  $M_S = 2 \rightarrow M_S = -2$  does not provide information regarding the separation between  $M_S$  levels

with different absolute quantum numbers, we were unable to extract zero-field splitting parameters from these data. However, the absence of observable allowed transitions in these spectra is not surprising given the large axial zero-field splitting parameters of these four  $[(\text{tpa}^{\text{R}})\text{Fe}]^{-}$  compounds relative to **5**. For instance, according to fits to the magnetization data, compound **4** exhibits the next smallest magnitude of  $D$  across the series, with  $D = -26(2) \text{ cm}^{-1}$ . The lowest-field allowed transition expected for a molecule with this value occurs at ca. 12 T at 224 GHz. Moreover, this transition is located ca. 100 K higher in energy than the corresponding  $\Delta M_S = 4$  transition at 12 T, which indicates that an experimental temperature of 100 K would be necessary to observe a peak. Unfortunately, data obtained at such a high temperature show a very low signal/noise ratio, such that any peak in the spectrum is likely lost in the background.

### Concluding Remarks

In summary, we have described the synthesis and properties of a novel family of nonheme trigonal pyramidal iron(II) pyrrolide complexes exhibiting considerable magnetic anisotropy and slow magnetic relaxation. These coordinatively unsaturated high-spin  $S = 2$  iron(II) compounds have been characterized by X-ray crystallography, static and dynamic magnetic susceptibility measurements, Mössbauer spectroscopy, and high-field EPR spectroscopy. Through systematic modification of a conserved three-fold symmetric trispyrrolide  $[\text{tpa}^{\text{R}}]^{3-}$  core with sterically demanding alkyl and aryl substituents, we reveal a range of large uniaxial zero-field splittings and relaxation barriers for the corresponding  $[(\text{tpa}^{\text{R}})\text{Fe}]^{-}$ . In addition, high-field EPR measurements provide direct independent evidence for negative zero-field splittings in this mononuclear high-spin iron(II) platform. Moreover, through the use of more sterically encumbering and more Lewis basic alkyl pendants to prevent distortions from three-fold symmetry and engender stronger axial anisotropy, we have successfully increased the barrier to spin inversion up to  $U_{\text{eff}} = 65 \text{ cm}^{-1}$  for compound **1**. Taken together, these studies establish the first class of mononuclear transition metal complexes in which slow magnetic relaxation has been observed, and the collective structural and spectroscopic data provide a starting point for further studies into the reactivity and magnetic properties of this promising family of bioinspired coordination compounds.

### Experimental Section

**Synthetic Materials and Methods.** Unless otherwise noted, all manipulations were carried out at room temperature under an atmosphere of dinitrogen in a Vacuum Atmospheres glovebox or using Schlenk techniques. Pentane, dimethoxyethane (DME), tetrahydrofuran (THF), and diethyl ether were deoxygenated by sparging with dinitrogen and dried via Vacuum Atmospheres solvent purification system. Diisopropyl ether was distilled from purple sodium/benzophenone ketyl. Dry 1,2-dichloroethane was purchased from Acros, and  $\text{FeCl}_2$  beads were purchased from Strem. Potassium hydride was purchased as a suspension in mineral oil, washed with pentane, and used as a dry solid inside the glovebox. Literature procedures were used for the preparation of ethyl pyrrole-2-carboxylate (**6**),<sup>95</sup>  $\text{K}[(\text{tpa}^{\text{Mes}})\text{Fe}]$  (**2**),<sup>69</sup> tris((5-phenyl-1*H*-pyrrol-2-yl)methyl)amine ( $\text{H}_3\text{tpa}^{\text{Ph}}$ ) (**7**),<sup>69</sup> and tris((5-(2,4,6-triisopropylphenyl)-1*H*-pyrrol-2-yl)methyl)amine ( $\text{H}_3\text{tpa}^{\text{Triip}}$ ) (**8**).<sup>74</sup> All other reagents and solvents were purchased from chemical suppliers and used as received. NMR spectra were recorded on Bruker spectrometers

operating at 300 or 400 MHz as noted. Chemical shifts are reported in ppm and referenced to residual protiated solvent; coupling constants are reported in Hz. Mass spectra and elemental analyses were performed at the Mass Spectrometry and Microanalytical Facilities at the University of California, Berkeley.

**Magnetic Measurements.** Magnetic data were collected using a Quantum Design MPMS-XL SQUID magnetometer. Measurements for **1–5** were obtained for finely ground microcrystalline powders restrained in a frozen eicosane matrix within polycarbonate capsules. Dc susceptibility measurements were collected in the temperature range 2–300 K under a dc field of 1000 Oe. Dc magnetization measurements were obtained in the temperature range 1.8–10 K under dc fields of 1, 2, 3, 4, 5, 6, and 7 T. These data were fit in the temperature range 1.8–3.0 K. In general, several different values of  $E$  could be obtained and had little to no effect on the goodness-of-fit, depending only on the input values for  $E$ . As such, only the maximum values of  $E$  are reported. In addition, in cases where multiple fits of similar quality provided slightly different values of  $D$ , the average value is reported with the standard deviation given in parentheses. Values of  $g$  are reported to only two significant figures to be consistent with  $D$  values and to account for any small errors in sample weighing. Ac susceptibility measurements were obtained in the temperature range 1.7–6.8 K under a 4 Oe ac field oscillating at frequencies of 1–1488 Hz, under an applied dc field of 1500 Oe. Dc magnetic susceptibility data were corrected for diamagnetic contributions from the sample holder and eicosane, as well as for the core diamagnetism of each sample (estimated using Pascal's constants).

**Mössbauer Spectroscopy.** The Mössbauer spectra of compounds **1**, **2**, and **4** have been measured between 4.2 and 220, 280, and 250 K, respectively, in a Janis Superveritemp cryostat with a constant-acceleration spectrometer that utilized a rhodium matrix cobalt-57 source and was calibrated at 295 K with  $\alpha$ -iron powder. The Mössbauer spectral absorbers of **1**, **2**, and **4** contained 60(5), 85(5), and 35(5)  $\text{mg}/\text{cm}^2$ , respectively, of powder mixed with boron nitride; the errors are high because of the difficulty of preparing the absorbers under an inert atmosphere. The statistical errors are given in parentheses in the text and tables. However, more realistic absolute errors for the isomer shifts are  $\pm 0.005 \text{ mm/s}$ , for the quadrupole shifts and line widths are  $\pm 0.01 \text{ mm/s}$ , and for the relative component areas are  $\pm 1\%$ .

**General Methods for X-ray Crystallography.** Crystals were mounted on Kapton or monofilament loops in Paratone-N hydrocarbon oil. Air-sensitive samples were transferred from the glovebox to Paratone-N and mounted quickly to avoid decomposition. All data collection was performed on a Bruker (formerly Siemens) SMART diffractometer/CCD area detector equipped with a low temperature apparatus. Data integration was performed using SAINT. Preliminary data analysis and absorption correction were performed with the Bruker APEX2 software package. Structure solution by direct methods was performed using SIR2004,<sup>96</sup> and the resulting solution was refined using SHELX. Hydrogen atoms were included in calculated positions.<sup>97</sup> Details of the data collection and refinement for **1**, **2**, **4**, and **5** can be found in Table 3.

**High-Field Electron Paramagnetic Resonance Spectroscopy.** High-field, high-frequency EPR spectra at temperatures ranging from ca. 3 to 290 K were recorded on a home-built spectrometer at the Electron Magnetic Resonance facility of National High Magnetic Field Laboratory. The setup of this instrument has been described in detail previously. The instrument is a transmission-type device in which microwaves are propagated in cylindrical lightpipes. The microwaves are generated by a phase-locked Virginia Diodes source, generating a frequency of  $13 \pm 1 \text{ GHz}$  and producing its harmonics of which the 2nd, 4th, 6th, 8th, 16th,

(95) Bailey, D. M.; Johnson, R. E.; Albertson, N. F. *Org. Synth.* **1988**, 50–9, 618.

(96) Burla, M. C.; Caliendo, R.; Camalli, M.; Carrozzini, B.; Cascarano, G. L.; De Caro, L.; Giacovazzo, C.; Polidori, G.; Spagna, R. *J. Appl. Crystallogr.* **2005**, 38, 381.

(97) Sheldrick, G. M. *Acta Crystallogr., Sect. A: Found. Crystallogr.* **2008**, 64, 112.

**Table 3.** Experimental Details for the X-ray Structures of Complexes **1**, **2**, **4**, and **5**

	1	2 <sup>a</sup>	4	5
formula	C <sub>31</sub> H <sub>47</sub> N <sub>4</sub> ONaFe	C <sub>58</sub> H <sub>85</sub> N <sub>4</sub> O <sub>8</sub> KFe	C <sub>45</sub> H <sub>57</sub> N <sub>4</sub> O <sub>6</sub> NaFe	C <sub>49</sub> H <sub>61</sub> N <sub>4</sub> O <sub>8</sub> F <sub>6</sub> KFe
formula weight	570.57	1061.28	828.79	1042.97
<i>T</i> (K)	128(2)	141(2)	123(2)	153(2)
$\lambda$ (Å)	0.71069	0.71069	0.71069	0.71069
crystal system	cubic	monoclinic	triclinic	orthorhombic
space group	<i>P</i> 2 <sub>1</sub> 3 (#198)	<i>P</i> 2 <sub>1</sub> / <i>c</i> (#14)	<i>P</i> 1 (#2)	<i>P</i> 2 <sub>1</sub> 2 <sub>1</sub> 2 <sub>1</sub> (#19)
<i>a</i> (Å)	14.7696(3)	17.625(5)	11.3600(17)	13.467(2)
<i>b</i> (Å)	14.7696(3)	13.840(4)	12.0280(18)	18.827(4)
<i>c</i> (Å)	14.7696(3)	24.177(6)	17.8810(26)	20.082(4)
$\alpha$ (deg)	90	90	76.897(2)	90
$\beta$ (deg)	90	95.855(4)	73.871(2)	90
$\gamma$ (deg)	90	90	69.850(2)	90
<i>V</i> (Å <sup>3</sup> )	3221.86(1)	5867(2)	2190.03(21)	5091.7(16)
<i>Z</i>	4	4	2	4
$\rho_{\text{calcd}}$ (g/cm <sup>3</sup> )	1.18	1.20	1.26	1.36
$\mu$ (mm <sup>-1</sup> )	0.509	0.382	0.407	0.455
<i>F</i> (000)	1224	2280	880	2184
reflectns collected	18416	26424	16928	33040
ind reflectns ( <i>R</i> <sub>int</sub> )	2223 (0.028)	6050 (0.032)	8139 (0.030)	10400 (0.061)
<i>T</i> <sub>min</sub> / <i>T</i> <sub>max</sub>	0.87	0.85	0.92	0.88
data/restr/params	2223/0/130	6287/0/649	8139/0/520	10400/0/630
<i>R</i> , <i>R</i> <sub>w</sub> , <i>R</i> <sub>all</sub>	0.028, 0.076, 0.031	0.040, 0.047, 0.077	0.063, 0.070, 0.12	0.048, 0.092, 0.086
GOF	1.10	1.66	1.01	0.98
max shift/error	0.01	0.00	0.07	0.01

<sup>a</sup> Data taken from ref 70.

24th, and 32nd are available. A superconducting magnet (Oxford Instruments) capable of reaching a field of 17 T was employed.

**Least-Squares Fitting of the High-Field EPR Data.**<sup>98</sup> The program used to fit the multifrequency data calculated the energies of the sublevels within the *S* = 2 spin ground state through diagonalization of the spin Hamiltonian matrix using the Householder transformation.<sup>99</sup> The resonance fields at each orientation of the magnetic field defined by the polar angles  $\Theta$  and  $\Phi$  were found by using an iterative procedure. Our instrument employs no resonance cavity; thus, we observe resonances caused by microwaves whose *B*<sub>microwave</sub> is parallel to *B*<sub>magnet</sub> in addition to the usual EPR transitions, owing to the poorly defined microwave modes. Upon finding by trial and error method the initial parameters *g*, *D*, and *E*, all transitions observed in all experimental powder spectra were identified as corresponding to the X, Y, or Z orientations. A table whose rows contained frequency,  $\Theta$ ,  $\Phi$ , and resonance field was used as input data. The program attempted to minimize the function:

$$\chi^2 = \sum_{i=1}^N (f_i^{\text{(calc)}} - f_i^{\text{(exp)}})^2$$

by use of the Simplex method. After convergence had been achieved, the Hessian matrix was calculated. The Hessian matrix is formally a matrix containing the second derivatives of  $\chi^2$  with respect to parameters *p*:

$$H_{ij} = \frac{\delta^2 \chi^2}{\delta p_i \delta p_j}$$

but, as it is generally done, it was calculated from:

$$H_{ij} = \sum_{k=1}^N \left( \frac{\delta f_k^{\text{calc}}}{\delta p_i} \right) \left( \frac{\delta f_k^{\text{calc}}}{\delta p_j} \right)$$

The derivatives of the resonance fields,  $f_k^{\text{calc}}$ , with respect to the parameters *p*, had to be evaluated numerically. Finally, errors in the best-fit parameters were estimated as:

$$\sigma_i = \sqrt{\frac{\chi^2}{N - P} (H^{-1})_{ii}}$$

where *N* is the number of experimental resonance fields and *P* is the number of fitted parameters.

**Ethyl 5-*tert*-Butylpyrrole-2-carboxylate (9).** This compound was prepared by the modification of a literature procedure.<sup>100</sup> A dry, round-bottom flask was charged with a stir bar, **6** (30.0 g, 0.216 mol), and 2 L of anhydrous 1,2-dichloroethane. The flask was purged with dinitrogen, and AlCl<sub>3</sub> (60.5 g, 0.454 mol) was added in one portion followed by the immediate addition of 2-chloro-2-methylpropane (23.7 mL, 0.216 mol). The resulting mixture was stirred under nitrogen for 2 h and then quenched in air by careful addition to a saturated solution of aqueous NaHCO<sub>3</sub> (2 L). Diethyl ether (1 L) was added and the organic layer separated. The aqueous layer was then further extracted with ether (2 × 250 mL). The combined organic portions were dried over anhydrous Na<sub>2</sub>SO<sub>4</sub> and concentrated by rotary evaporation to yield a pale brown oil which crystallized upon standing to give 37.5 g (89%) of an off-white solid which was used without further purification. The spectral properties of this material were identical to those reported in the literature.<sup>101</sup>

**2-*tert*-Butylpyrrole (10).** A slurry of **9** (65.5 g, 0.335 mol) and powdered NaOH (67.0 g, 1.68 mol) in ethylene glycol (650 mL) was brought to reflux with the aid of a heating mantle. After 6 h, the reaction mixture was allowed to cool to room temperature, diluted with water (800 mL), and extracted with CH<sub>2</sub>Cl<sub>2</sub> (5 × 200 mL). The organic portions were dried over anhydrous Na<sub>2</sub>SO<sub>4</sub> and concentrated by rotary evaporation to yield a brown oil which was vacuum distilled into a flask cooled to -78 °C to give 35.0 g (85%)

- (98) Aromi, G.; Telsler, J.; Ozarowski, A.; Brunel, L. C.; Stoeckli-Evans, H. M.; Krzystek, J. *Inorg. Chem.* **2005**, *44*, 187.  
 (99) Wilkinson, J. H. *The algebraic eigenvalue problem*; Oxford University Press, USA, 1988.

- (100) Wood, J. E.; Wild, H.; Rogers, D. H.; Lyons, J.; Katz, M.; Caringal, Y.; Dally, R.; Lee, W.; Smith, R. A.; Blum, C. U.S. Patent 6,187,799, 2001.  
 (101) Elder, T.; Gregory, L. C.; Orozco, A.; Pflug, J. L.; Wiens, P. S.; Wilkinson, T. J. *Synth. Commun.* **1989**, *19*, 763.

of a colorless crystalline solid. The spectral properties of this material were identical to those reported in the literature.<sup>102</sup>

**Tris(5-*tert*-butyl-1*H*-pyrrol-2-ylmethyl)amine, H<sub>3</sub>tpa<sup>t-Bu</sup> (6).** To a solution of NH<sub>4</sub>Cl (1.50 g, 28.0 mmol) in an ethanol/water mixture (1:1 v/v, 60 mL) was added aqueous formaldehyde (37 wt %, 6.80 g, 83.7 mmol) followed by a solution of **10** (10.3 g, 83.7 mmol) in ethanol (30 mL). The resulting mixture was stirred for three days at room temperature under nitrogen at which point a fine white precipitate was collected by filtration, washed with a small portion of ethanol, briefly air-dried, and dissolved in CH<sub>2</sub>Cl<sub>2</sub> (200 mL). The solution was washed with 20% aqueous NaOH (200 mL) and the aqueous layer extracted further with CH<sub>2</sub>Cl<sub>2</sub> (2 × 100 mL). The organic portions were combined, dried over anhydrous Na<sub>2</sub>SO<sub>4</sub>, and concentrated to a pale yellow oil that was dried in vacuo to give a pale yellow foam. The foam was triturated with 5 mL of hexanes and filtered to yield 7.1 g (60%) of the title compound as a fine white powder. <sup>1</sup>H NMR (400 MHz, CDCl<sub>3</sub>): δ 8.13 (s, 3 H), 5.94 (t, *J* = 2.8 Hz, 3 H), 5.84 (t, *J* = 2.8 Hz, 3 H), 3.52 (s, 6 H), 1.30 (s, 9 H); <sup>13</sup>C NMR (CDCl<sub>3</sub>, 100 MHz) δ 142.1, 126.7, 107.7, 102.3, 49.8, 31.6, 30.8.

**Na[(tpa<sup>t-Bu</sup>)Fe]·THF (1).** To a solution of **11** (664 mg, 1.57 mmol) in THF (10 mL) was added solid NaN(SiMe<sub>3</sub>)<sub>2</sub> (865 mg, 4.71 mmol). After the mixture was stirred for 2 h, the volatiles were removed under reduced pressure, and the colorless residue was redissolved in THF (10 mL). Solid FeCl<sub>2</sub> (199 mg, 1.57 mmol) was added and the resulting slurry stirred for 6 h. Precipitated NaCl was removed by filtration over Celite, and the filtrate was concentrated under reduced pressure to a colorless glaze. Redissolution of this residue in minimal THF followed by layering with pentane deposited colorless tetrahedral crystals which were washed with pentane and dried in vacuo to yield 456 mg (51%) of a microcrystalline solid. Anal. Calcd for C<sub>31</sub>H<sub>47</sub>FeN<sub>4</sub>NaO: C, 65.26; H, 8.30; N, 9.79. Found: C, 64.83; H, 8.43; N, 9.55.

**K[(tpa<sup>Trip</sup>)Fe]·3 DME (3).** To a stirring solution of **8** (514 mg, 0.597 mmol) in THF (10 mL) was added solid KH (144 mg, 3.59 mmol) in ca. 10 portions, resulting in vigorous effervescence. After the mixture was stirred for 2 h, effervescence had ceased and the slurry was filtered to remove excess KH. Solid FeCl<sub>2</sub> (76 mg, 0.60 mmol) was added to the filtrate, and the resulting slurry was stirred for 6 h. Precipitated KCl was removed by filtration over Celite, and the filtrate was concentrated under reduced pressure to a colorless glaze. Dissolving this residue in minimal 1:1 DME/*i*-Pr<sub>2</sub>O and layering with pentane deposited colorless, block-shaped crystals which were washed with pentane and dried in vacuo to yield 490 mg (67%) of a white powder. Anal. Calcd for C<sub>72</sub>H<sub>111</sub>FeKN<sub>4</sub>O<sub>6</sub>: C, 70.67; H, 9.14; N, 4.58. Found: C, 70.44; H, 9.31; N, 4.81.

**Na[(tpa<sup>Ph</sup>)Fe]·3 DME (4).** To a stirring solution of **7** (486 mg, 1.01 mmol) in THF (10 mL) was added solid NaH (145 mg, 604 mmol) in ca. 10 portions, resulting in vigorous effervescence. After the mixture was stirred for 2 h, effervescence had ceased and the slurry was filtered to remove excess NaH. Solid FeCl<sub>2</sub> (128 mg, 1.01 mmol) was added to the filtrate, and the resulting slurry was stirred for 6 h. Precipitated NaCl was removed by filtration over Celite, and the filtrate was concentrated under reduced pressure to a yellow glaze. Dissolution of this residue in a minimal amount of THF followed by layering with DME deposited yellow crystals which were washed with DME and dried in vacuo to afford 475 mg (57%) of yellow, microcrystalline solid. Anal. Calcd for C<sub>45</sub>H<sub>57</sub>FeN<sub>4</sub>NaO<sub>6</sub>: C, 65.21; H, 6.93; N, 6.76. Found: C, 65.14; H, 6.91; N, 6.86.

**2-(2,6-Difluorophenyl)-1*H*-pyrrole (15).** This compound was prepared by the modification of a literature procedure.<sup>73</sup> In the glovebox, sodium pyrrole (1.35 g, 15.2 mmol), ZnCl<sub>2</sub> (2.07 g, 15.2 mmol), and THF (35 mL) were combined in a heavy-walled reaction vessel and allowed to stir for 5 min. (Caution: vigorously exothermic.) Then 2-(di-*tert*-butylphosphino)biphenyl (31.1 mg,

0.104 mmol), Pd<sub>2</sub>dba<sub>3</sub> (17.4 mg, 0.0190 mmol), and 1-bromo-2,6-difluorobenzene (0.974 g, 5.05 mmol) were added sequentially. The reaction vessel was sealed, removed from the glovebox, and heated in an oil bath at 100 °C for 48 h. After the mixture was cooled to ambient temperature, diethyl ether (100 mL) and water (100 mL) were added to the reaction, and the dark mixture was filtered through Celite, washing the residue with diethyl ether (30 mL). The organic portion of the filtrate was separated and the aqueous layer extracted further with diethyl ether (3 × 75 mL). The combined organic portions were dried over Na<sub>2</sub>SO<sub>4</sub> and concentrated by rotary evaporation. Purification of the resultant residue by column chromatography on silica gel (5% ethyl acetate/hexanes) provided 0.485 g (54%) of the title compound as a slightly orange oil. The spectral properties of this material were identical to those reported in the literature.<sup>103</sup>

**Tris(5-(2,6-difluorophenyl)-1*H*-pyrrol-2-yl)methyl)amine, H<sub>3</sub>tpa<sup>DFP</sup> (16).** To a solution of NH<sub>4</sub>Cl (0.183 g, 3.42 mmol) in an ethanol/water mixture (1:1 v/v, 20 mL) was added 37 wt % aqueous formaldehyde (0.836 g, 10.3 mmol) followed by a solution of **15** (1.84 g, 10.3 mmol) in ethanol (15 mL). The resulting mixture was stirred for three days at room temperature under nitrogen at which point a fine white precipitate was collected by filtration, washed with a small portion of ethanol, briefly air-dried, and dissolved in CH<sub>2</sub>Cl<sub>2</sub> (100 mL). The solution was washed with 20% aqueous NaOH (100 mL) and the aqueous layer extracted further with CH<sub>2</sub>Cl<sub>2</sub> (2 × 75 mL). The organic portions were combined, dried over anhydrous Na<sub>2</sub>SO<sub>4</sub>, and concentrated to a colorless oil that crystallized on standing to yield 0.661 g (33%) of a colorless solid. <sup>1</sup>H NMR (400 MHz, CDCl<sub>3</sub>): δ 9.23 (s, 3 H), 7.08 (m, 3 H), 6.97 (t, *J* = 22 Hz, 6 H), 6.84 (s, 3 H), 6.27 (s, 3 H) 3.71 (s, 6 H); <sup>13</sup>C NMR (CDCl<sub>3</sub>, 100 MHz) δ 159.3 (dd, *J* = 9, 246 Hz), 130.1 (s), 125.8 (t, *J* = 12 Hz), 120.6 (s), 112.6 (s), 112.2 (d, *J* = 27 Hz), 110.6 (t, *J* = 15 Hz), 109.52 (s), 50.0 (s); <sup>19</sup>F (CDCl<sub>3</sub>, 376 MHz) δ -112.6 (s). HRFABMS ([M + 1]<sup>+</sup>) *m/z* calcd for C<sub>33</sub>H<sub>25</sub>N<sub>4</sub>F<sub>6</sub> 591.1983, found 591.1985.

**K[(tpa<sup>DFP</sup>)Fe]·2 DME (5).** To a stirring solution of **16** (698 mg, 1.18 mmol) in THF (10 mL) was added solid KH (284 mg, 7.09 mmol) in ca. 10 portions resulting in vigorous effervescence. After the mixture was stirred for 2 h, effervescence had ceased and the slurry was filtered to remove excess KH. Solid FeCl<sub>2</sub> (150 mg, 1.18 mmol) was added to the filtrate, and the resulting slurry was stirred for 6 h. Precipitated KCl was removed by filtration over Celite, and the filtrate was concentrated under reduced pressure to a yellow glaze. Dissolution of this residue in a minimal amount of DME followed by layering with pentane deposited yellow crystals which were washed with pentane and dried in vacuo to afford 575 mg (56%) of a yellow powder. Anal. Calcd for C<sub>41</sub>H<sub>41</sub>N<sub>4</sub>O<sub>4</sub>F<sub>6</sub>KFe: C, 57.08; H, 4.79; N, 6.49. Found: C, 57.29; H, 4.56; N, 6.58.

**Acknowledgment.** We thank the Packard foundation (C.J.C.), DOE/LBNL (403801 to C.J.C.), the NSF (CHE-0617063 to J.R.L.), and the FNRS-Belgium (9.456595 and 1.5.064.05 to F.G.) for funding this work. We also thank Arkema (W.H.H.) as well as Tyco Electronics (T.D.H. and D.E.F.) for graduate fellowship support. C.J.C. is an Investigator with the Howard Hughes Medical Institute. The NHMFL is funded by the NSF through the Cooperative Agreement No. DMR-0654118, the State of Florida, and the DOE. F.G. thanks Prof. R. Cloots for the use of his controlled atmosphere glove box.

**Supporting Information Available:** Additional magnetic data, Mössbauer spectra and experimental details. This information is available free of charge via the Internet at <http://pubs.acs.org>.

JA105291X

(102) Spaggiari, A.; Vaccari, D.; Davoli, P.; Prati, F. *Synthesis* **2006**, 995.

(103) Kruse, C. G.; Bouw, J. P.; Vanhes, R.; Vandekuilten, A.; Denhartog, J. A. *J. Heterocycles* **1987**, *26*, 3141.